Wiley
Journal of Food Biochemistry
Volume 2025, Article ID 9941885, 16 pages
https://doi.org/10.1155/jfbc/9941885

WILEY

Research Article

Identification of Polyphenols in *Mallotus peltatus* (Geiseler) Mull. Arg. Based on UPLC-MS/MS and Their Protective Effects on H_2O_2-Induced Liver Injury

Ying-Jing Zhang,[1] Jin-Xin Li,[2] Ke-Xin Hao,[1] Rui-Fang Zhong,[1] Yi-Meng Li,[1,3] Jian-Guo Jiang,[1] and Wei Zhu[2]

[1]*College of Food and Bioengineering, South China University of Technology, Guangzhou, China*
[2]*The Second Affiliated Hospital, Guangzhou University of Chinese Medicine, Guangzhou, China*
[3]*Dermatology Hospital of Southern Medical University, Guangzhou, China*

Correspondence should be addressed to Jian-Guo Jiang; jgjiang@scut.edu.cn and Wei Zhu; zhuwei9201@163.com

Received 10 January 2025; Accepted 14 March 2025

Academic Editor: Ignazio Restivo

Copyright © 2025 Ying-Jing Zhang et al. Journal of Food Biochemistry published by John Wiley & Sons Ltd. This is an open access article under the terms of the Creative Commons Attribution License, which permits use, distribution and reproduction in any medium, provided the original work is properly cited.

Background: Liver cells are particularly susceptible to mitochondrial dysfunction due to external stimuli, leading to excess reactive oxygen species (ROS) and redox imbalance. The aim of this study was to extract and purify the polyphenolic fractions of *Mallotus peltatus* (Geiseler) Mull. Arg. and evaluate their potential protective effect against H_2O_2-induced oxidative stress injury in hepatocytes.
Methods: The extraction process of polyphenols in MPMA was optimized by the response surface method. Then, we purified the crude extracts with macroporous resin HPD600 to obtain MPMAP-I, MPMAP-II, and MPMAP-III. The physical properties and component composition of the samples were analyzed by FT-IR and UPLC-MS/MS. An in vitro H_2O_2-induced oxidative stress injury model in hepatocytes was established to investigate the protective effect of MPMAP-I on L02 cells. The effect was assessed by measuring cell survival rate, enzyme activities, intracellular ROS levels, cell apoptosis rate, mitochondrial membrane potential, and the mRNA expression of related signaling pathways.
Results: The results showed that the optimized extraction conditions of MPMA were 60% ethanol, 140 min, 85°C, and liquid-to-solid ratio of 30 mL/g. All three purified fractions contained different polyphenols (such as kaempferol 3-O-sophoroside, corilagin, and cirsiliol) and had great antioxidant activities. MPMAP-I treatment could increase the activities of SOD, CAT, and GPx in H_2O_2-induced L02 cells, reduce the content of MDA, the activities of transaminases, the production of intracellular ROS, and the rate of cell apoptosis, and restore mitochondrial function. Furthermore, these effects might be related to the inactivation of the Bcl2/Bax/caspase-3 apoptotic pathway and the activation of the Nrf2/γ-GCL antioxidant pathway.
Conclusion: Our study provided a theoretical basis for the protective effect of MPMA polyphenols on liver injury, which is helpful to improve the development and application of MPMA in medicine and healthcare products.

Keywords: liver injury; *Mallotus peltatus* (Geiseler) Müll. Arg.; oxidative stress; polyphenols

1. Introduction

Nonalcoholic fatty liver disease (NAFLD) is a common chronic liver disease, which can cause a variety of pathologies such as obesity, dyslipidemia, diabetes mellitus, insulin resistance, hypertension, nonalcoholic steatohepatitis (NASH), cirrhosis, and cardiovascular disease [1]. Over the past decade, the incidence of NAFLD has dramatically increased worldwide, particularly in developing countries, and it has been reported in 46% of the middle-aged population in the United States [2, 3]. Studies have found that mitochondrial diseases are closely related to liver cell function.

Mitochondria regulate the redox of hepatocytes, enabling the liver to maintain normal lipid homeostasis. An imbalance between excessive mitochondrial reactive oxygen species (ROS) production and the antioxidant system can lead to liver dysfunction and NAFLD [2]. Therefore, NAFLD is closely related to cellular oxidative stress. Many antioxidants and antioxidant substances have been shown to protect the liver from oxidative stress and injury, which further supports the association between oxidative stress and liver injury [4–6]. By emphasizing the potential role of antioxidants in the prevention or treatment of NAFLD, this research provides theoretical support for subsequent studies.

Polyphenols are secondary metabolites found in most plants and have been shown to play a protective role in liver health by combating oxidative stress [7]. For instance, resveratrol has been reported to alleviate NAFLD by acting as an anti-ROS agent, mitigating DNA damage through the p53/p21 signaling pathway [8]. Additionally, studies using three animal models of NAFLD/NASH demonstrated that black soybean polyphenols can prevent the progression of these conditions by reducing oxidative stress and inhibiting liver lipid accumulation [9]. Furthermore, polyphenols from blueberry leaves can alleviate NAFLD by improving mitochondrial dysfunction and oxidative defense, thereby reducing hepatic steatosis, oxidative stress, and inflammatory response [10]. Notably, higher intakes of total polyphenols, phenolic acids, and lignin were associated with a lower probability of developing NAFLD, emphasizing the potential importance of a diet rich in polyphenols to help reduce NAFLD and its risk of progression to advanced stages [11]. The synergistic effects of various active compounds, particularly natural polyphenols, present new therapeutic strategies for addressing NAFLD.

Mallotus peltatus (Geiseler) Müll. Arg. (MPMA), a member of the Euphorbia family, is widely distributed in Southeast Asia and Hainan Province, China [12–14]. This plant is known locally as "glossy ganoderma grass" in Hainan, representing a vital economic commodity as well as traditional medicine [15]. MPMA is rich in bioactive compounds, including polysaccharides, fatty acids, triterpenoids, polyphenols, and alkaloids, which contribute to its numerous biological activities. For example, purified polysaccharides from MPMA exhibit excellent free radical scavenging and α-glucosidase inhibitory activities [14]. Additionally, bioactive fraction A and isolated ursolic acid from MPMA have demonstrated antiviral properties by inhibiting the early stages of herpes simplex virus replication [12]. Research has also identified the antimicrobial, anti-inflammatory [13], antiatherosclerotic [16], and antiobesity effects of MPMA, as well as its potential to improve central nervous system function [17] and alleviate gastric mucosal injury [15]. Despite these promising medicinal and economic values, research on MPMA, particularly regarding its hepatoprotective effects, remains limited.

Oxidative stress and liver damage are critical health issues, often associated with chronic diseases and environmental factors. To optimize the yield of MPMA active substances, we employed the response surface method (RSM), focusing on total phenolic content (TPC) as a key parameter. This strategy was complemented by infrared spectroscopy to explore structural differences among the purified components. Our comprehensive analysis, using six different in vitro methods, provided a unique assessment of the antioxidant activities of these components. Additionally, by establishing an H_2O_2-induced oxidative stress model in L02 cells and employing quantitative real-time PCR, we explored the antioxidative stress capability and liver-protective effects of the sample, making progress in the molecular pathways involved in oxidative stress and apoptosis. This work not only provides valuable insights into the bioactive properties of MPMA but also offers references for future studies on the mechanisms underlying its protective effects against oxidative stress and liver damage.

2. Materials and Methods

2.1. Plant Materials and Reagents. The leaves of MPMA were collected from Ding'an County, Hainan Province, and were identified by Professor Gang Hao (College of Life Science, South China Agriculture University). The voucher specimen of MPMA (No. SKC211007) has been deposited in the College of Food Science and Engineering, South China University of Technology. The leaves of MPMA natural were dried, ground into powder, and sieved through a 60-mesh sieve. The powder was stored in sealed bags for further experimentation.

Dulbecco's modified Eagle's medium (DMEM) was provided by Gibco. Fetal bovine serum (FBS) and phosphate-buffered saline (PBS) were provided by VivaCell Biosciences (Shanghai, China). The BCA protein concentration assay kit (P0009), total superoxide dismutase (SOD) assay kit with WST-8 (S0101), catalase (CAT) assay kit (S0051), total glutathione peroxidase (GPx) assay kit with DTNB (S0059S), malondialdehyde (MDA) assay kit (S0131), ROS assay kit (S0033), Annexin V-FITC apoptosis detection kit (C1062), and enhanced mitochondrial membrane potential (MMP) assay kit with JC-1 were purchased from Beyotime Biotechnology (Shanghai, China). Glutamic oxaloacetic transaminase (GOT) assay kit (C010-2-1) and glutamic pyruvic transaminase (GPT) assay kit (C009-2-1) were obtained from Nanjing Jiancheng Bioengineering Institute (Nanjing, China). The EZ-press RNA purification kit (B0004DP), color reverse transcription kit (with gDNA remover) (A0010CGQ), and 2× color SYBR green qPCR master mix (A0012-R1) were obtained from EZBioscience (USA). All other chemicals used were of analytical grade.

2.2. Optimization of Extraction Conditions

2.2.1. Single-Factor Design of Polyphenols. Single-factor experiments were designed with reference to previous studies [18–20]. As shown in Supporting Table S1, four factors (extraction time, temperature, liquid-to-solid ratio, and ethanol concentration) affecting the TPC in the ethanol extraction of MPMA were explored. The TPC of the MPMA extractions was measured using the Folin–Ciocalteu's colorimetric method [18] with minor modification. Briefly, 10–60 μg/mL gallic acid standard solution was prepared, and

after the extract was diluted 35 times, 1 mL standard solution or sample solution was mixed with 5 mL Folin–Ciocalteu's solution (10% v/v) for 5 min, respectively. Subsequently, 4 mL Na_2CO_3 (7.5% w/v) was added, and after 60 min of reaction at room temperature in the dark, the absorbance was measured at 760 nm using a UV spectrophotometer (Shanghai Scientific Instrument Co., LTD. UV754N, China). The results are expressed in milligrams of gallic acid equivalent per gram dry weight (mg GAE/g dw) of MPMA. The standard curve is shown in equation (1):

$$Y = 0.0105C - 0.0053, \quad (1)$$

where Y represents the absorbance of the diluted sample at 760 nm and C (μg/mL) represents the concentration of polyphenol in the sample.

$$\text{The TPC yield of sample (mg/g)} = \frac{C \times V \times N}{M}, \quad (2)$$

where C (μg/mL) is the concentration of polyphenol in the sample, V (mL) is the total volume of the extract, N is the dilution ratio, and M (g) is the dry weight of the sample.

2.2.2. Response Surface Optimization. Based on the results of a single-factor experiment, three factors, including extraction time (A), temperature (B), and liquid-to-solid ratio (C), with significant responses to TPC were chosen as independent variables, and TPC was considered the response value. The extraction conditions were optimized using the RSM, and 17 experimental combinations were analyzed using Design-Expert (Supporting Table S2) [18].

2.2.3. Extraction and Purification of Polyphenols. According to the results of RSM, the MPMA were extracted by 60% ethanol, 140 min, 85°C, and liquid-to-solid ratio of 30 mL/g. The extraction was concentrated by a rotary evaporator and purified by macroporous resin HPD600 with water and different concentrations of ethanol to obtain the polyphenols from MPMA. Then, solutions were concentrated and dried at 60°C, through the determination of TPC content. The 30%, 50%, and 70% elution fractions were named MPMAP-I, MPMAP-II, and MPMAP-III, and the TPC contents were 423, 413, and 228 mg/g, respectively. Figure 1 shows the specific operation process.

2.3. FT-IR Characterization. For analyzing the structure of samples, the MPMAP-I, MPMAP-II, and MPMAP-III were mixed with KBr, pressed, and measured in a Fourier infrared spectrometer (Thermo Fisher Nicolet IS50, USA) to obtain spectra. The scanning range was 4000–500 cm^{-1} [21].

2.4. UPLC-MS/MS Analysis. The components of MPMAP-I, MPMAP-II, and MPMAP-III were analyzed using a UPLC-MS/MS system (Agilent1290/Bruker maXis impact). The mobile phase consisted of acetonitrile (A) and ultrapure water (B). The gradient elution program was as follows: 5% (A) for 0–2 min; 5%–100% (A) from 2 to 20 min; 100% (A) from 20 to 24 min; and back to 5% (A) from 24 to 30 min. The column temperature was maintained at 35°C, with a flow rate of 0.25 mL/min and an injection volume of 20 μL. The mass spectrometer was equipped with an electrospray ionization (ESI) source, and detection was performed in the negative ion mode. The capillary voltage was set to 3500 V, with a gas flow rate of 4.0 L/min and a scan range of 50–1500 m/z.

2.5. Antioxidant Activities

2.5.1. $ABTS^{\cdot+}$ Scavenging Ability. The scavenging effect against $ABTS^{\cdot+}$ of MPMAP-I, MPMAP-II, and MPMAP-III was determined by a 96-well microplate using a modified version of the previous method [22]. After the ABTS stock solution was prepared, ABTS solutions with different concentrations were obtained by dilution with absolute ethanol, and their absorbance at 734 nm was measured by a UV spectrophotometer (Shanghai Scientific Instrument Co., LTD. UV754N, China). The concentration selected for the experiment was 0.2626 mM. 180 μL of ABTS solutions and 20 μL of sample solutions (50–800 μg/mL) were added to each well. After mixing, the reaction was carried out in the dark at 30°C for 6 min. Distilled water and VC solution were used to replace the sample solution as blank and positive controls, respectively.

The $ABTS^{\cdot+}$ scavenging rate of the sample was calculated as shown in equation (3):

$$\text{radical scavenging rate (\%)} = \frac{A_c - A_s}{A_c} \times 100, \quad (3)$$

where A_c and A_{sS} are the absorbance at a certain wavelength of the control and the sample, respectively.

2.5.2. DPPH· Scavenging Ability. The scavenging ability against DPPH· was determined by the 96-well microplate method [22]. Distilled water and VC solution were used to replace the sample solution as blank and positive controls, respectively. The DPPH· scavenging rate of the sample was calculated as shown in equation (3).

2.5.3. ·OH Scavenging Ability. The ·OH scavenging ability was determined by the 96-well microplate method [23]. The experiment was performed in the dark. Distilled water and VC solution were used to replace the sample solutions as blank and positive controls, respectively. The ·OH radical scavenging rate of the sample was calculated as shown in equation (3).

2.5.4. $\cdot O_2^-$ Scavenging Ability. The $\cdot O_2^-$ scavenging ability was determined by the 96-well microplate method [24] with minor modification. 150 μL Tris–HCl buffer solution (0.05 mM, pH = 8.0) and 30 μL sample solutions (50–800 μg/mL) were mixed, and then, the plate was incubated in the dark at room temperature for 10 min. Next, 30 μL pyrogallol solution (6 mM) was added, mixed with slight shaking, and left in the dark at room temperature for 10 min. Finally,

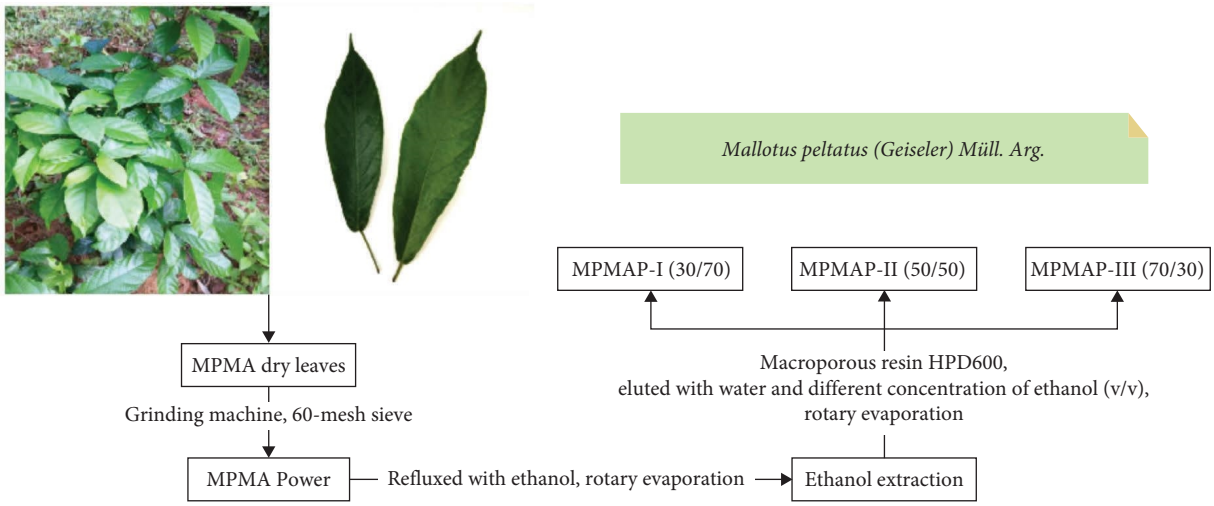


Figure 1: MPMA extraction process.

30 μL of 8 mM HCl solution was added to terminate the reaction, and the absorbance was measured at 325 nm. Distilled water and VC solution were used to replace the sample solution as blank and positive controls, respectively. The $\cdot O_2^-$ scavenging rate of the sample was calculated as shown in equation (3).

2.5.5. Ferric Reducing Antioxidant Power (FRAP). The FRAP was determined by the 96-well microplate method [22]. 0.083 mM TPTZ working solution was prepared, and then, 20 μL ferrous sulfate solution with different concentrations and 180 μL TPTZ working solution were added to the 96-well plate. After the reaction at 37°C in the dark for 10 min, the absorbance was measured at 596 nm to establish an absorbance–concentration standard curve of ferrous sulfate. The concentration of mM representing the same absorbance as ferrous sulfate is the FRAP value of the sample. Distilled water and VC solution were used to replace the sample solution as blank and positive controls, respectively.

2.5.6. Total Reducing Power. The total reducing power was determined by the 96-well microplate method [23]. Briefly, 40 μL samples at various concentrations (50–800 μg/mL) were mixed with 100 μL of phosphate buffer (0.2 M, pH 6.6) and 100 μL of $K_3Fe(CN)_6$ solution (1%, w/v). The mixtures were then reacted at 50°C for 20 min. Then, 100 μL of CCl_3COOH solution (10%, w/v) was added to shut down the reaction. Subsequently, 100 μL of supernate was mixed with 100 μL of distilled water and 20 μL of $FeCl_3$ solution (0.1%, w/v) in the 96-well plate. Ten minutes later, the plate was shaken sufficiently and measured spectrophotometrically at 700 nm. Distilled water and VC solution were used to replace the sample solution as blank and positive controls, respectively. The total reducing power of the sample was calculated as equation (4):

$$\text{total reducing power} = A_S - A_C, \tag{4}$$

where A_C and A_S are the absorbance at a certain wavelength of the control and the sample, respectively.

2.6. Effects on H_2O_2-Induced L02 Cells

2.6.1. Cell Culture and Cytotoxicity Assay. L02 cells were cultured in DMEM with 10% FBS and 1% penicillin–streptomycin (referred to as complete medium) and maintained at 37°C in a 5% CO_2 incubator. The passage number of L02 cells used in the experiments did not exceed 15.

The cytotoxicity was assessed using the MTT assay [25] with some modifications as reflected. L02 cells were seeded at a density of 5×10^3 cells/mL in 96-well plates and cultured for 24 h. When the count of cells was appropriate, the old culture medium from each well was removed, the cells were washed twice with PBS, and the cells were treated with different concentrations of MPMAP-I, MPMAP-II, and MPMAP-III (0, 25, 50, 100, 200, and 400 μg/mL, 24 h) or H_2O_2 (50, 100, 200, 400, 600, 800, and 1000 μM, 4 h). The concentration of H_2O_2 at which the survival rate of the injury group was around 50% was selected as the modeling condition for subsequent experiments [26, 27].

To evaluate the effects of the samples on the viability of H_2O_2-induced L02 cells, the cells were treated with the samples for 24 h and then induced with H_2O_2 for 4 h followed by MTT assay.

MTT solution (5 mg/mL) prepared in PBS (stored at 4°C) was diluted 10-fold with DMEM high glucose medium to prepare the MTT working solution. After certain treatment, cells were incubated with MTT working solution for 4 h, followed by the addition of DMSO to dissolve the purple formazan crystals. The optical density (OD) was measured at 490 nm using a microplate reader (Tecan Infinite 200, Switzerland). The viability of L02 cells was calculated according to equation (5):

$$\text{the viability of L02 cells}\,(\%) = \frac{A_S}{A_C} \times 100. \tag{5}$$

2.6.2. Determination of Intracellular Antioxidant Enzymes and MDA Content. After 4 h of H_2O_2 treatment, the cells and culture medium were collected, and the enzyme activities of SOD, CAT, GPx, and the content of MDA were measured according to the instructions of the relevant kit [27, 28].

2.6.3. Determination of Intracellular Transaminase Content. After 4 h of H_2O_2 treatment, the cells and culture medium were collected, and the enzyme activities of GOT and GPT were measured according to the instructions of the relevant kit [28].

2.6.4. Measurement of Intracellular ROS, Apoptosis Rate, and MMP. ROS detection was performed using the fluorescent probe DCFH-DA. Intracellular ROS can oxidize non-fluorescent DCFH to produce fluorescent DCF. Detection of DCF fluorescence can be used to know the level of intracellular ROS. During early apoptosis, phosphatidylserine (PS) is transferred from the inner to the outer side of the cell membrane and exposed on the cell surface. Annexin V is a protein capable of binding PS with high affinity, and when combined with fluorescein isothiocyanate (FITC), it can detect cells with PS eversion by flow cytometry. JC-1 is a fluorescent dye that assesses cell injury or apoptosis by detecting changes in MMP. In healthy cells, JC-1 forms red fluorescent aggregates in the mitochondria. When apoptosis occurs, the membrane potential drops, leading to green fluorescence. The red-to-green fluorescence ratio is used to evaluate the extent of injury or apoptosis.

After 4 h of H_2O_2 treatment, the cells and culture medium were collected, and intracellular ROS and apoptosis rate were measured by flow cytometry (NovoCyte Quanteon, USA), and MMP was measured by inverted fluorescence microscopy (Nikon, Japan) according to the instructions of the relevant kit [28, 29].

2.6.5. Quantitative Real-Time PCR (qRT-PCR) Assay. After 4 h of H_2O_2 treatment, the cells and culture medium were collected, total RNA was extracted following the manufacturer's instructions, and the concentration and purity of RNA were measured by a spectrophotometer (NanoDrop 2000 c, USA). The cDNA was synthesized by reverse transcription using the reverse transcription kit [29].

qRT-PCR amplification reactions: Follow the instructions of the 2 × color SYBR green qPCR master mix kit. 20 μL reaction system (10 μLSYBR Green Master + 6 μL DEPC water + 2 μL cDNA + 2 μL primer) was used to detect the effect of samples on the expression of related genes in L02 cells. The results were normalized to the expression of β-actin, and the primers for the genes are shown in Supporting Table S3.

2.7. Statistical Analysis. All experiments were repeated at least three times independently, and the data were expressed as mean ± standard deviation. Data were analyzed by one-way ANOVA using the SPSS 25 statistical analysis program followed by Tukey's multiple comparisons. $^{*}p < 0.05$ was considered significant and $^{**}p < 0.01$ was considered extremely significant. All data results were graphically analyzed using Origin 2021 software.

3. Results and Discussion

3.1. Single-Factor Design of Polyphenols. The TPC yield of MPMA gradually increased with the extension of extraction time from 30 to 150 min, reaching a maximum of 127.86 mg/g around 150 min. When the extraction time exceeded 150 min, the TPC yield decreased (Figure 2(a)). It was speculated that the solvent volatilization was caused by too long heating time, which affected the dissolution of polyphenols [30].

Besides, with the increase in extraction temperature, the TPC yield of MPMA gradually increased and reached a maximum value of 126.33 mg/g near 80°C (Figure 2(b)). Because heating energy can reduce viscosity and surface tension by disrupting cell structure, thereby improving extraction efficiency [31]. However, excessive temperature might cause some polyphenols to undergo chemical reactions, resulting in structural changes [32].

Additionally, Figure 2(c) shows that the TPC yield of MPMA could reach 119.05 mg/g when the liquid-to-solid ratio was 25 mL/g. The appropriate increase in extraction solvent could help the solvent to fully extract the sample and increase the dissolution of polyphenols. When the solvent was too much, the dissolved polyphenols reached the upper limit, but the solvent diluted the content of polyphenols [32]. Higher or lower ethanol concentration was not conducive to improving the TPC yield of MPMA.

When the ethanol concentration was between 40% and 60%, the TPC yield of MPMA was significantly increased, and the yield reached the maximum when the ethanol concentration was about 60%. After increasing the ethanol concentration, the boiling point of the system was gradually reduced, and the solvent evaporation speed became faster, which may lead to the fact that TPC could not be completely extracted. In addition, the polarity of ethanol aqueous solvent decreases with the increase of ethanol concentration [33], which showed that the polarity of phenolic compounds in MPMA was low, and the dissolution effect is good at 60% ethanol concentration. The TPC yield of MPMA decreased significantly when ethanol concentration exceeded 60%. (Figure 2(d)).

Among them, because the ethanol concentration had no significant effect on the TPC yield of MPMA, 150 min, 80°C, and 25 mL/g were selected for the subsequent study.

3.2. Optimization of Extraction Conditions. Central composite design and results of the TPC yield of MPMA are shown in Supporting Table S2. Table 1 shows the ANOVA to assess the significance of the fit of the regression model to the experimental data. The model F-value of 39.22 implied the model was significant. The quadratic regression model was significant ($p < 0.05$), while the lack of fit was not significant ($p > 0.05$), indicating that the model was reliable in calculating TPC. The predicted R^2 of 0.8449 was in reasonable

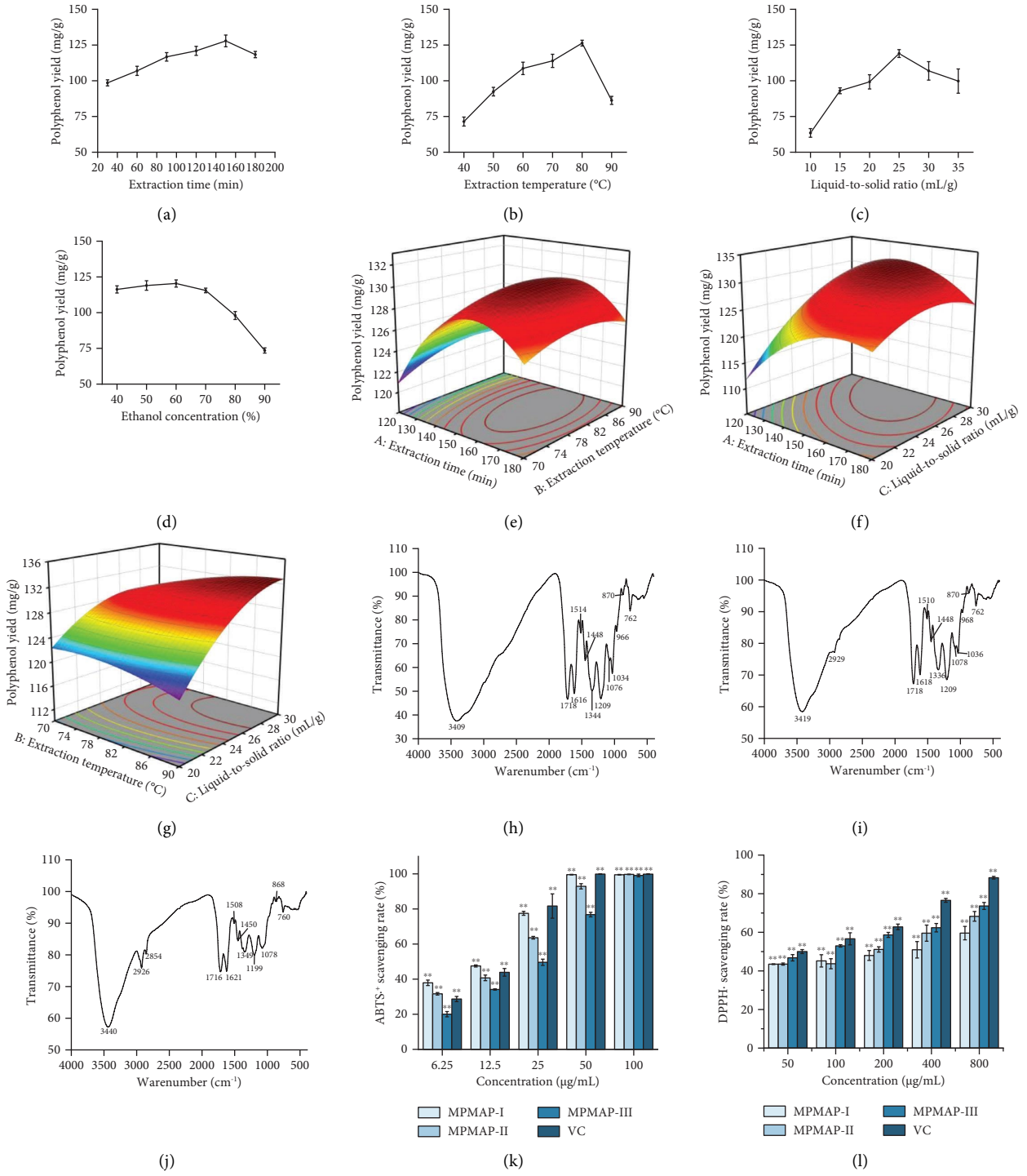


Figure 2: Continued.

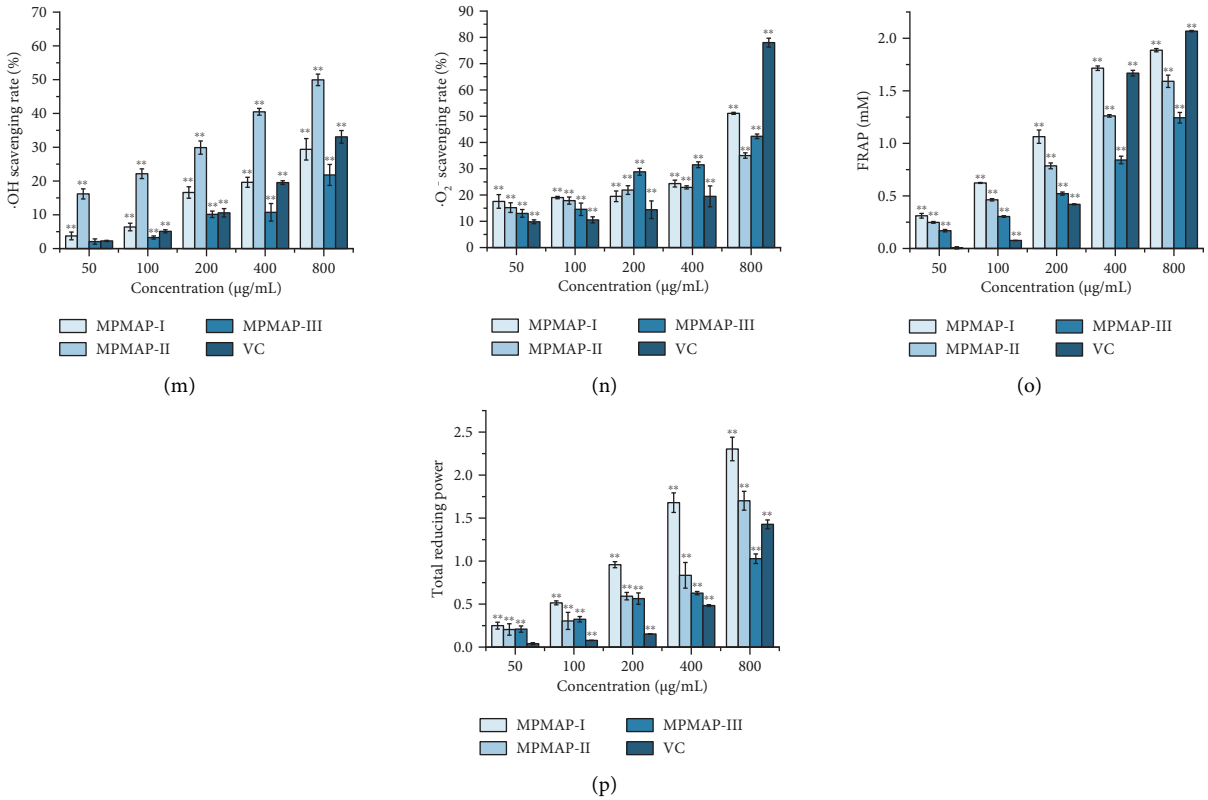


Figure 2: Optimization of extraction conditions, FT-IR spectra, and antioxidant activities of MPMAP-I, MPMAP-II, and MPMAP-III. Effects of extraction time (a), temperature (b), liquid-to-solid ratio (c), and ethanol concentration (d) on the TPC yield of MPMA. 3D response surface plots of the TPC yield of MPMA in terms of extraction time vs temperature (e), time vs liquid-to-solid ratio (f), temperature vs liquid-to-solid ratio (g). FT-IR spectra of MPMAP-I (h), MPMAP-II (i), and MPMAP-III (j). ABTS·$^+$ (k), DPPH· (l), ·OH (m), ·O_2^- (n) scavenging rate, FRAP (o), and total reducing power (p) of MPMAP-I, MPMAP-II and MPMAP-III, respectively. $^{**}p < 0.01$, compared with the control group, the difference was statistically significant.

Table 1: Analysis of the variance of the fitted quadratic regression models.

Source	Sum of squares	df	Mean square	*F*-value	*p* value	
Model	438.32	9	48.7	39.22	< 0.0001	
A	36.12	1	36.12	29.09	0.001	
B	3.14	1	3.14	2.53	0.1559	
C	173.82	1	173.82	139.99	< 0.0001	
AB	0.6972	1	0.6972	0.5615	0.4781	
AC	52.93	1	52.93	42.62	0.0003	Significant
BC	13.4	1	13.4	10.79	0.0134	
A^2	98.63	1	98.63	79.44	< 0.0001	
B^2	5.64	1	5.64	4.54	0.0705	
C^2	41.58	1	41.58	33.49	0.0007	
Residual	8.69	7	1.24			
Lack of fit	3.86	3	1.29	1.07	0.4572	
Pure error	4.83	4	1.21			
Cor total	447.01	16				Not significant
R^2	0.9806					
Adjusted R^2	0.9556					
CV (%)	0.8863					

agreement with the adjusted R^2 of 0.9556. Moreover, the coefficient of variation (CV) was less than 10%, which manifested the good precision and reproducibility of the model.

According to the F-value, the order of influence of extraction conditions on TPC is C (liquid/solid ratio) > A (time) > B (temperature). The response diagram of the regression equation is shown in Figures 2(e), 2(f), and 2(g).

The significant terms in the model equation were linear terms of A and C and quadratic terms of AC, BC, A^2, and C^2 (Table 1). The quadratic model of the response was expressed as follows:

$$\begin{aligned} Y_{TPC} = {} & 130.02 + 2.12A + 0.6262B + 4.66C \\ & - 0.4175AB - 3.64AC + 1.83BC \\ & - 4.84A^2 - 1.16B^2 - 3.14C^2. \end{aligned} \quad (6)$$

The optimal extraction conditions were 139.939 min, 83.5544°C, and 29.4195 mL/g liquid-to-solid ratio, and the TPC yield was estimated to be 132.207 mg/g. According to the needs of practical application, the specific extraction conditions of subsequent sample was adjusted to 60% ethanol, 140 min, 85°C, and 30 mL/g liquid-to-solid ratio.

3.3. FT-IR Characterization. As FT-IR spectra are shown in Figures 2(h), 2(i), and 2(j), three samples had polyphenol characteristic absorption peaks, consistent or close to each other, with dense absorption peaks from 1800 to 500 cm^{-1}. The broad and strong absorption of MPMAP-I at 3409 cm^{-1} was caused by O–H stretching vibration, indicating that there may be phenolic hydroxyl groups in the sample [34]. The peaks at 1344, 966, 870, and 762 cm^{-1} corresponded to the bending vibration of C–H, where 966, 870, and 762 cm^{-1} were the out-of-plane bending vibration of C–H [35, 36]. The peak at 1718 cm^{-1} was a bending vibration of C=O, indicating that the sample may contain flavonoids [34]. The peaks at 1616, 1514, and 1448 cm^{-1} were the C=C stretching vibration on the benzene ring [21, 37], and the peaks at 1209 and 1034 cm^{-1} were the C–O stretching vibration, which might be the phenolic group [36, 37].

Similar to MPMAP-1, MPMAP-II and MPMAP-III also had O–H stretching vibration, C–H bending vibration, C=O bending vibration, C=C stretching vibration, and C–O stretching vibration. The corresponding peaks are shown in Table 2, and the shift of some absorption peaks might be due to the difference in the specific structure of the polyphenol in the samples.

3.4. The Components of MPMAP-I, MPMAP-II, and MPMAP-III. As shown in Supporting Figure S1(A–C), the retention time and peak area of MPMAP-I, MPMAP-II, and MPMAP-III were different, indicating that the macroporous resin HPD600 could be used to separate the compounds, which made the composition differences among the three samples evident. As shown in Table 3, the main chemical constituents of MPMAP-I, MPMAP-II, and MPMAP-III were polyphenols. However, with the exception of MPMAP-I and MPMAP-II, which both contained 6,4′-dimethoxyisoflavone-7-glucoside (Wistin), the other components varied, further indicating that the crude extracts were well separated. Notably, MPMAP-I and MPMAP-II contained a greater variety of polyphenolic compounds. Specifically, MPMAP-I contained swertiajaponin, kaempferol 3-O-sophoroside, epihesperidin, ficuflavoside, guaijaverin, 8-prenylnaringenin, and 6,4′-dimethoxyisoflavone-7-glucoside (Wistin), while MPMAP-II contained corilagin, hesperetin-7-O-rutinoside, biflavonoid-flavone base + 3O, flavone base + 2O + 1MeO, 3-O-neohesperidoside kaempferol, luteolin-6-C-glucoside, silychrystin, 6,4′-dimethoxyisoflavone-7-glucoside (Wistin), and cynarin. In contrast, MPMAP-III had relatively fewer polyphenols, including Procyanidin B1, hesperidin, cirsiliol, scutellarein-7-glucuronide, and feruloyl hexoside (isomer of 849). These polyphenols exhibit excellent antioxidant and anti-inflammatory effects, and their natural activities will play an important role in subsequent experiments.

3.5. Antioxidant Activity

3.5.1. $ABTS^{\cdot+}$ Scavenging Ability. $ABTS^{\cdot+}$ are dark radicals that accept hydrogen radicals or electrons to form molecules with a discoloration effect [22]. As shown in Figure 2(k), the effect of MPMAP-I on scavenging $ABTS^{\cdot+}$ was close to that of VC, and MPMAP-I > MPMAP-II > MPMAP-III. The scavenging activity of $ABTS^{\cdot+}$ from all three samples was concentration-dependent and consistent with that of positive control VC at 100 μg/mL.

3.5.2. DPPH· Scavenging Ability. ·DPPH, as a kind of stable free radical, has a single electron, so it can accept an electron or hydrogen ion and has a maximum absorption at a wavelength of 517 nm. In the presence of free radical scavengers, the single electron of DPPH is captured and its color becomes lighter. The decrease of absorbance level indicates the increase of antioxidant capacity, so as to evaluate the antioxidant capacity of the test sample [24]. In Figure 2(l), the DPPH· scavenging effect of MPMAP-III was better than that of MPMAP-II and MPMAP-I. From 50 to 800 μg/mL, DPPH· scavenging rates were 46.81%–73.65%, 43.54%–68.27%, and 43.49%–59.59%, respectively. However, the effect of the three was slightly weaker than that of VC.

3.5.3. ·OH Scavenging Ability. ·OH are the most active type of ROS, which can react with all neighboring biomolecules, such as lipids, proteins, and carbohydrates, leading to various diseases [23]. ·OH scavenging effect was ranked as MPMAP-II > MPMAP-I > MPMAP-III, all showing a concentration dependence. Among them, MPMAP-II was more effective than VC, and the clearance rate of ·OH was 16.18%–49.95% at 50–800 μg/mL (Figure 2(m)).

3.5.4. $\cdot O_2^-$ Scavenging Ability. The scavenging activity of $\cdot O_2^-$ was concentration-dependent for all three samples (Figure 2(n)). At the concentration of 50–400 μg/mL, the $\cdot O_2^-$ scavenging rates of the three samples were higher than that of the corresponding concentration of VC, but at 800 μg/mL, the $\cdot O_2^-$ scavenging rates of the three samples were 51.08% (MPMAP-I), 35.03% (MPMAP-II), and 42.35% (MPMAP-III), respectively, lower than that of VC.

Table 2: Vibration absorption peaks and corresponding functional groups of MPMAP-1, MPMAP-II, and MPMAP-III.

Sample	Wavenumber (cm^{-1})				
	O–H	C–H	C=O	C=C (Aromatic)	C–O
MPMAP-I	3409	1344, 966, 870, 762	1718	1616, 1514, 1448	1209, 1034
MPMAP-II	3419	2929, 1336, 968, 870, 762	1718	1618, 1510, 1448	1209, 1078, 1036
MPMAP-III	3440	2926, 2854, 1349, 868, 760	1716	1621, 1508, 1450	1199, 1078

3.5.5. FRAP. Under acidic conditions, Fe^{3+} forms a complex with TPTZ, in which ferric ions are reduced to divalent ions by reducing agents, and the solution changes from yellow to bright blue [22]. The FRAP values of MPMAP-I were all higher than those of VC at 50–400 μg/mL and slightly lower than that of VC at 800 μg/mL. Similarly, the FRAP values of MPMAP-II and MPMAP-III at low concentrations were also higher than those of VC, and the FRAP values increased as the sample concentration increased (Figure 2(o)).

3.5.6. Total Reducing Power. In the concentration range of 50–800 μg/mL, the total reducing power of MPMAP-I and MPMAP-II was greater than that of VC. The total reducing power of the three samples was ranked as MPMAP-I > MPMAP-II > MPMAP-III (Figure 2(p)).

3.6. MPMAP-I Inhibited the Hepatotoxicity of L02 Cells Induced by H_2O_2. In order to explore the cytotoxicity of MPMAP-I, MPMAP-II, and MPMAP-III, L02 cells were treated with different concentrations for 24 h and detected by MTT assay. As shown in Figure 3(a), MPMAP-I, MPMAP-II, and MPMAP-III showed no obvious cytotoxicity to L02 cells. The viability of L02 cells treated by MPMAP-III, ranging from 79.49% to 90.08%, was lower than those of the other two samples.

Next, L02 cells were incubated in different concentrations of H_2O_2 (50–1000 μM) for 4 h. As shown in Figure 3(b), H_2O_2 exposure resulted in a dose-dependent decrease in the viability of L02 cells. Compared with the control group, the survival rate of L02 cells at 800 μM H_2O_2 was 51.76%. Therefore, 800 μM H_2O_2 was used to establish the L02 cell damage model.

Afterward, as shown in Figure 3(c), MPMAP-I at the concentration of 25–400 μg/mL could effectively increase the viability of H_2O_2-induced L02 cells by 23.75%–39.29% compared with the control group in a dose-dependent manner. At 100–400 μg/mL, MPMAP-II and MPMAP-III also had a better effect on cell viability, but not as obvious as MPMAP-I. Therefore, the further experimental investigation would be conducted for MPMAP-I.

3.7. MPMAP-I Alleviated L02 Cells Oxidative Stress and Hepatocellular Injury Induced by H_2O_2. The activities of SOD, CAT, GPx, content of MDA, and activities of GOT and GPT were determined to evaluate the antioxidant and liver protective effects of MPMAP-I on H_2O_2-induced oxidative stress in L02 cells.

As shown in Figures 3(d), 3(e), and 3(f), the activities of SOD, CAT, and GPx in the model group were significantly lower than those in the control group, indicating that H_2O_2 damage increased the level of oxidative stress in the cells. After treatment with different concentrations of MPMAP-I, the activities of SOD, CAT, and GPx in the cells were increased to varying degrees. Compared with the model group, the activities of SOD and CAT (200 and 400 μg/mL MPMAP-I treatment) were significantly increased ($p < 0.01$) in a dose-dependent manner. Moreover, the activity of GPx was significantly improved after MPMAP-I treatment. 400 μg/mL MPMAP-I treatment could restore the activity of GPx to 0.16 U/mgprot, which was close to that of the control group (0.18 U/mgprot), but it was not dose-dependent. MDA is a product of lipid peroxidation, which is positively correlated with ROS level and can indirectly reflect the damage degree of cell membrane [26]. As can be seen from Figure 3(g), the MDA level of L02 cells significantly decreased from 1.58 μM/mgprot in the model group to 0.49 μM/mgprot after treatment with 200 μg/mL MPMAP-I. These results indicated that MPMAP-I could effectively relieve the oxidative stress of L02 cells induced by H_2O_2.

Aminotransferase GOT and GPT are the most commonly used indicators of liver function. They are mainly distributed in liver cells. If liver cells are damaged, the intracellular GOT and GPT will leak to the outside of the cell, and the increase in the extracellular level of the two is positively correlated with the degree of liver cell damage [38]. As shown in Figures 3(h) and 3(i), compared with the cells in the control group, the activities of GOT and GPT in the model group after H_2O_2-induced injury were significantly increased to 5.66 and 52.38 U/gprot, respectively ($p < 0.01$), indicating that the H_2O_2 damage model was successfully established. After the intervention with different concentrations of MPMAP-I, the activities of GOT decreased significantly compared with the model group. When MPMAP-I was 400 μg/mL, the activity of GOT decreased to 1.19 U/gprot at the lowest level, indicating that the repair effect on L02 cells was obvious. Similarly, MPMAP-I could significantly reduce the activity of GPT in a concentration-dependent way. It is noteworthy that when MPMAP-I was 400 μg/mL, the activity of GPT was reduced to 18.23 U/gprot, indicating that MPMAP-I could effectively prevent H_2O_2-induced damage to L02 cells.

3.8. Effect of MPMAP-I on Intracellular ROS and Apoptosis Rate. Excessive ROS attacks intracellular biological macromolecules, including proteins and nucleic acids, eventually leading to mitochondrial dysfunction and apoptosis [29, 39]. Part of the natural antioxidant helps to reduce the occurrence of ROS and protect cells from damage [28]. As shown in Figures 4(a) and 4(d), the ROS level of L02 cells in the model group was significantly increased after H_2O_2

Table 3: UPLC-MS/MS method for identifying the main chemical components of MPMAP-I, MPMAP-II, and MPMAP-III.

	No.	Analytes	Formula	RT (min)	Mass	Parent ions	Fragment ions	Class
MPMAP-I	1	Swertiajaponin	$C_{22}H_{22}O_{11}$	3.26	462.1160	461.0403	298.5099, 313.0442	Flavonoids
	2	Kaempferol 3-O-sophoroside	$C_{27}H_{30}O_{16}$	3.61	610.1530	609.1459	429.036, 609.1452	Flavonoids
	3	Epihesperidin	$C_{28}H_{34}O_{15}$	3.77	610.1897	609.1463	301.0368, 302.0368	Flavonoids
	4	Ficuflavoside	$C_{26}H_{28}O_{14}$	4.04	564.1480	563.1424	293.0471, 413.0884	Flavonoids
	5	Continentalic acid	$C_{20}H_{30}O_2$	4.53	302.2250	300.9985	226.9962, 300.9972	Diterpenoids
	6	(10E,15Z)-9,12,13-Trihydroxyoctadeca-10,15-dienoic acid	$C_{18}H_{32}O_5$	6.51	328.2250	327.2812	171.1099, 211.1318	Fatty acids and conjugates
	7	Pinellic acid	$C_{18}H_{34}O_5$	6.92	330.2410	329.2344	211.1314, 229.1417	Fatty acids and conjugates
	8	Guaijaverin	$C_{20}H_{18}O_{11}$	7.08	434.0850	433.2660	271.9941, 300.9941	Flavonoids
	9	Longistylin C	$C_{20}H_{22}O_2$	8.59	294.1620	293.1756	222.1545, 235.1313	Stilbenoids
	10	8-Prenylnaringenin	$C_{20}H_{20}O_5$	12.76	340.1311	339.1991	151.0115, 233.7543	Flavonoids
	11	Aesculinum	$C_{15}H_{16}O_9$	12.83	340.2840	339.2010	85.2253, 180.9650	Coumarins
	12	2-O-Sinapoyl malate	$C_{15}H_{16}O_9$	13.87	340.2840	339.2345	163.1153, 164.1251	Phenylpropanoid
	13	6,4′-Dimethoxyisoflavone-7-glucoside (Wistin)	$C_{23}H_{24}O_{10}$	15.05	460.1369	459.2911	283.1722, 284.1718	Flavonoids
MPMAP-II	1	Corilagin	$C_{27}H_{22}O_{18}$	0.69	634.0954	633.0614	300.9990, 463.0425	Phenolic acids
	2	Hesperetin-7-O-rutinoside	$C_{28}H_{34}O_{15}$	3.67	610.1898	609.1485	247.0242, 300.0283	Flavonoids
	3	Biflavonoid-flavone base+3O and flavone base+2O+1MeO	$C_{31}H_{20}O_{10}$	5.90	552.4910	551.2554	343.0475, 551.2472	Flavonoids
	4	3-O-Neohesperidoside kaempferol	$C_{27}H_{30}O_{15}$	6.79	594.1585	593.2668	211.1326, 300.0187	Flavonoids
	5	Luteolin-6-C-glucoside	$C_{21}H_{20}O_{11}$	7.69	448.3800	447.1346	365.2302, 399.2480	Flavonoids
	6	Glc-Glc-octadecatrienoyl-sn-glycerol (isomer 1) (PUT)	$C_{33}H_{56}O_{14}$	9.03	676.3670	675.3618	277.2151, 397.1376	Fatty acids and conjugates
	7	Silychrystin	$C_{25}H_{22}O_{10}$	9.48	482.4410	481.2603	253.2192, 308.3043	Flavonoids
	8	18-Beta-glycyrrhetinic acid	$C_{30}H_{46}O_4$	13.26	470.3396	469.3331	427.3509, 469.3326	Triterpenoids
	9	6,4′-Dimethoxyisoflavone-7-glucoside (Wistin)	$C_{23}H_{24}O_{10}$	14.99	460.1369	459.2895	283.1713, 284.1705	Flavonoids
	10	Cynarin	$C_{25}H_{24}O_{12}$	15.46	516.4550	515.3552	351.2335, 352.2309	Phenolic acids
MPMAP-III	1	Procyanidin B1	$C_{30}H_{26}O_{12}$	6.15	578.1424	577.1329	97.1308, 425.1983	Flavonoids
	2	Hesperitin	$C_{16}H_{14}O_6$	6.16	302.0790	300.9996	176.2030, 283.0177	Flavonoids
	3	Cirsiliol	$C_{17}H_{14}O_7$	6.29	330.0740	329.0307	314.0055, 315.0056	Flavonoids
	4	Anthraquinone base+1O, MeOH, 1MeO, O-Hex-Pen	$C_{27}H_{30}O_{14}$	8.30	578.5230	577.2721	275.2056, 295.2262	Anthraquinones
	5	Saikosaponin C	$C_{48}H_{78}O_{17}$	11.81	926.5239	925.5386	225.1141, 235.0787	Triterpenoids
	6	Gardnutine	$C_{20}H_{22}N_2O_2$	12.27	322.4080	321.2105	183.0187, 225.0503	Alkaloids
	7	Yohimbic acid	$C_{20}H_{24}N_2O_3$	12.44	340.4230	339.1980	183.0152, 183.0328	Alkaloids
	8	Fructose 1,6-diphosphate	$C_6H_{14}O_{12}P_2$	12.49	339.9961	339.2008	97.6994, 197.0216	Saccharides
	9	Isoreserpin	$C_{33}H_{40}N_2O_9$	14.63	608.6880	607.2548	307.1956, 418.0564	Alkaloids
	10	Scutellarein-7-glucuronide	$C_{21}H_{18}O_{12}$	15.07	462.0798	459.2906	283.1681, 284.1772	Flavonoids
	11	Feruloyl hexoside (isomer of 849)	$C_{16}H_{20}O_9$	15.12	356.3270	355.1581	355.1560, 355.3196	Phenolic acids
	12	Ginkgolide B	$C_{20}H_{24}O_{10}$	15.61	424.4020	423.3278	205.1851, 208.8839	Diterpenoids

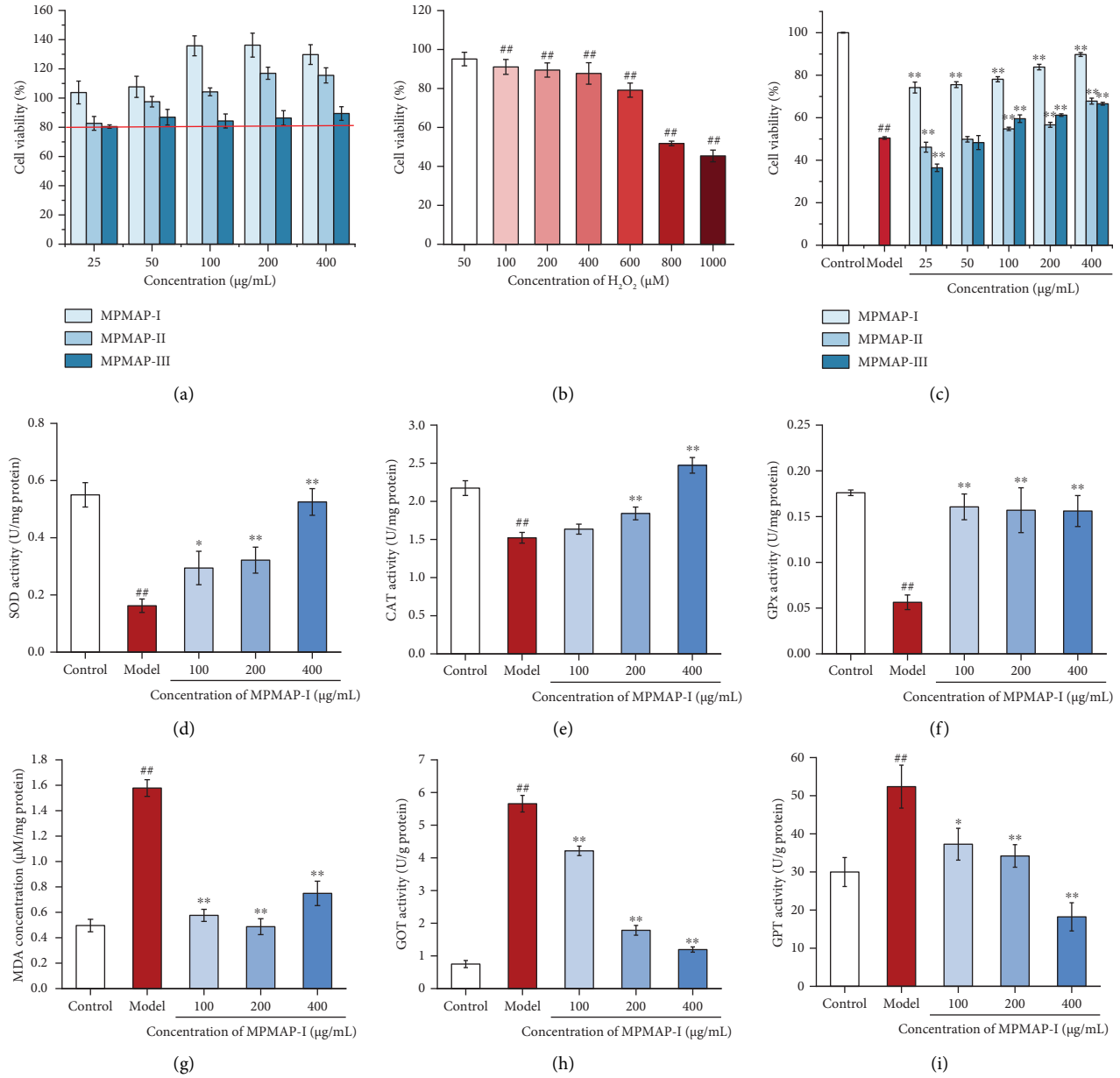


Figure 3: Effect of MPMAP-I, MPMAP-II, and MPMAP-III on H_2O_2-induced L02 cells, and MPMAP-I reduced H_2O_2-induced oxidative stress and the activities of transaminases. (a, b) The viability of L02 cells after treatment with various concentrations (25–400 μg/mL) of MPMAP-I, MPMAP-II, and MPMAP-III for 24 h or H_2O_2 (50–1000 μM) for 4 h, respectively, as detected by the MTT assay. (c–i) The cells were treated with different concentrations (100–400 μg/mL) of MPMAP-I for 24 h and then exposed to H_2O_2 (800 μM) for 4 h. The viability of cells was analyzed by the MTT assay (c). Effects of MPMAP-I on the activities of SOD (d), CAT (e), GPx (f), the content of MDA (g), and the activities of GOT (h) and GPT (i) in H_2O_2-treated L02 cells. $^{\#\#}p < 0.01$ compared with the control group; $^{*}p < 0.05$, $^{**}p < 0.01$, compared with the model group, the difference was statistically significant.

treatment, which was 2.16 times that of the control group. After treatment of MPMAP-I, the ROS level of L02 cells showed a dose-dependent decrease, and the ROS level after 200 μg/mL treatment was comparable to that of the control group, while the ROS level after 400 μg/mL treatment was 0.83 times of that of the control group. These results indicated that MPMAP-I could effectively reduce the ROS level in L02 cells and alleviate the oxidative stress damage caused by H_2O_2.

Cell apoptosis is shown in Figures 4(b) and 4(e). The four quadrants from the lower left to the upper left counterclockwise in each figure show cells in normal, early apoptotic, late apoptotic, and necrotic states, respectively. In the control group, the apoptosis rate of L02 cells was 2.27%, while in the model group, the apoptosis rate was significantly increased to 3.31%. After the addition of MPMAP-I intervention, the apoptosis rate decreased in a concentration-dependent manner, and the apoptosis rate of 400 μg/mL

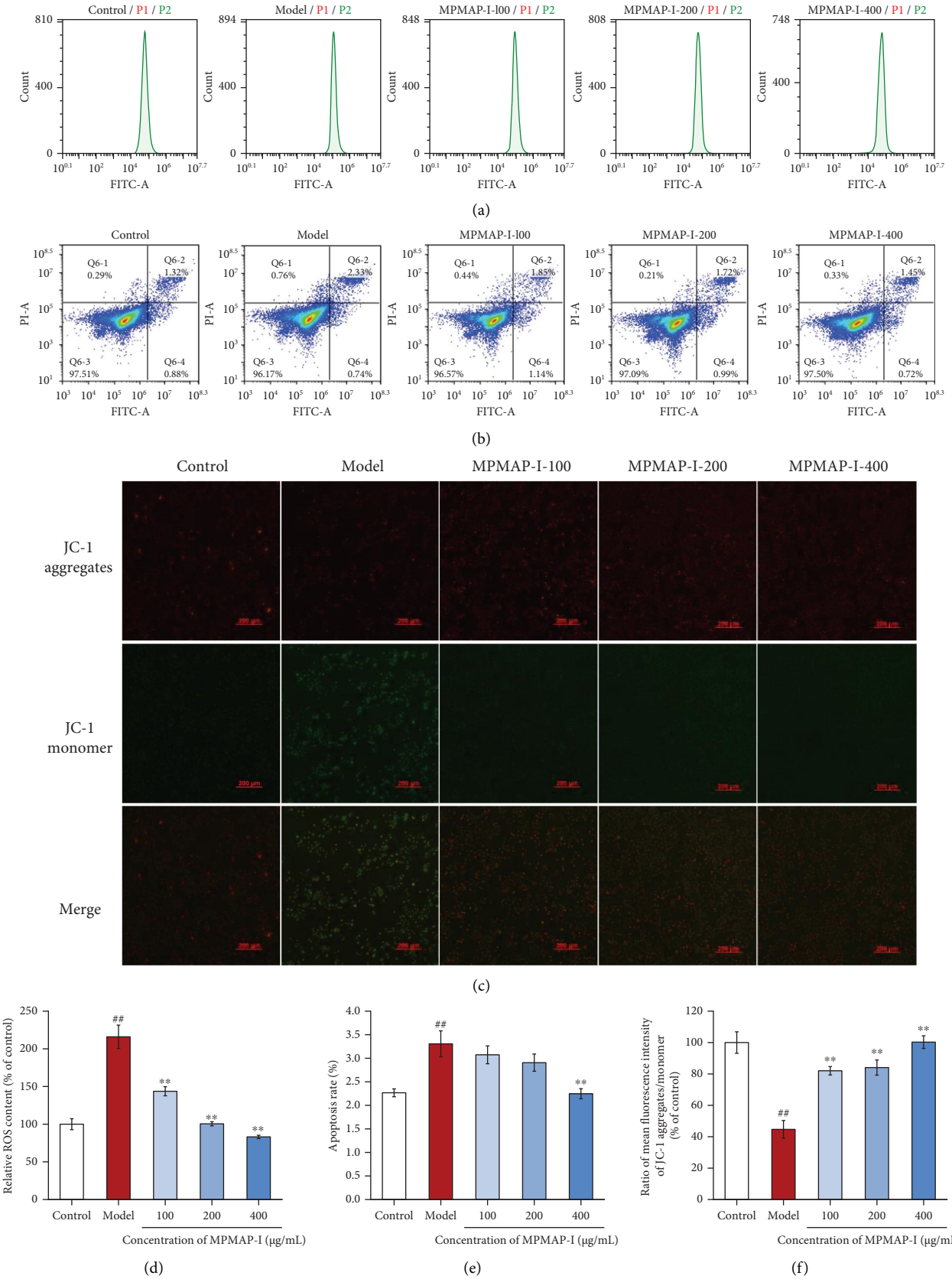


Figure 4: Detection of intracellular ROS, apoptosis rates, and MMP of L02 cells stimulated by H_2O_2. The cells were treated with different concentrations (100–400 μg/mL) of MPMAP-I for 24 h and then exposed to H_2O_2 (800 μM) for 4 h. (a) Flow cytometry analysis of intracellular ROS levels with DCFH-DA. (b) Flow cytometry analysis of apoptosis after double staining with Annexin V-FITC/PI. The upper right quadrants and the lower right quadrants represent number of the late apoptosis cells and early apoptosis cells, respectively. (c) MMP in JC-1-stained L02 cells, detected by inverted fluorescence microscopy. Scale bar = 200 μm. (d–f) Quantitative analysis of the mean DCF fluorescence intensity, the apoptosis rate in L02 cells, and the mean fluorescence intensity of JC-I aggregates/monomers. $^{\#\#}p < 0.01$ compared with the control group; $^{**}p < 0.01$, compared with the model group, the difference was statistically significant.

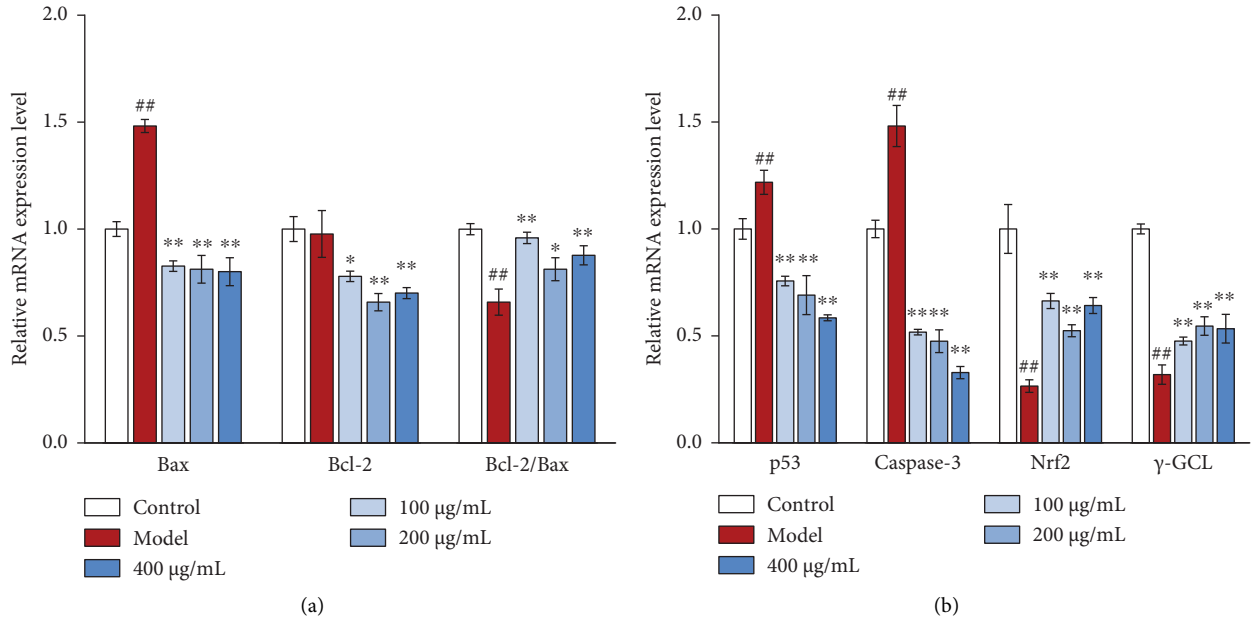


Figure 5: Effects of MPMAP-I on mRNA expression of apoptosis-related and oxidative stress–related genes in H_2O_2-injured L02 cells. The cells were treated with different concentrations (100–400 μg/mL) of MPMAP-I for 24 h and then exposed to H_2O_2 (800 μM) for 4 h. Relative mRNA levels of Bax, Bcl-2, Bcl-2/Bax (a), p53, caspase-3, Nrf2, and γ-GCL (b). $^{\#\#}p < 0.01$ compared with the control group; $^{*}p < 0.05$, $^{**}p < 0.01$, compared with the model group, the difference was statistically significant.

treatment was reduced to 2.25%, which was close to the control group and significantly different from the model group ($p < 0.01$).

3.9. MPMAP-I Restored MMP in H_2O_2-Induced L02 Cells. The change in MMP can be used as an early indicator of cell damage [29]. In order to explore the effect of MPMAP-I on MMP, the experiment adopted the JC-1 probe detection of L02 cell MMP. As shown in Figures 4(c) and 4(f), compared with the control group, the red fluorescence intensity of H_2O_2-treated L02 cells was decreased, and the green fluorescence intensity was significantly enhanced, indicating that the cells in the model group were subjected to oxidative damage and the MMP was decreased. However, after treatment with MPMAP-I, the ratio of red/green fluorescence level of L02 cells was higher than that of the model group, demonstrating that MPMAP-I could protect mitochondrial function and protect L02 cells from oxidative damage caused by H_2O_2.

3.10. mRNA Expression of Apoptosis and Oxidative Stress Genes. Existing research showed that the mitochondrial apoptosis pathway mediated damaged liver cell apoptosis [40]. Caspase-3 as the key enzyme of the mitochondrial apoptosis pathway could be activated in the early apoptosis, while the overexpression of p53 would activate downstream apoptotic genes accelerated apoptosis [41]. Oxidative stress is recognized as one of the important factors that lead to liver disease. Nrf2 is a key regulator of oxidative stress in a variety of cells including hepatocytes [42, 43]. In order to investigate the mechanism of apoptosis in H_2O_2-induced L02 cells, the mRNA expressions of Bax, Bcl-2, p53, and caspase-3 were analyzed by qRT-PCR.

As shown in Figure 5(a), the mRNA expression level of Bax was significantly increased, and the ratio of Bcl-2/Bax was significantly decreased in the model group. However, after MPMAP-I intervention, Bax mRNA expression was observably decreased while the ratio of Bcl-2/Bax was significantly increased, but no significant dose–effect relationship was found. In addition, compared with the control group, H_2O_2 induction also notably upregulated the mRNA expression levels of p53 and caspase-3, while the mRNA expression levels of MPMAP-I treatment were significantly decreased, even lower than those of the control group (Figure 5(b)). It can be seen from the above results that MPMAP-I could inhibit p53 overexpression, increase the ratio of Bcl-2/Bax, two key genes in the downstream of p53 mediating mitochondrial apoptosis pathway, and finally interfere with the cascade activation of caspase-3, thereby inhibiting apoptosis caused by H_2O_2 injury.

Plus, the mRNA expressions of Nrf2 and γ-GCL in the model group were significantly decreased, while the expressions of the corresponding genes were significantly upregulated after MPMAP-I treatment (Figure 5(b)). These results suggested that MPMAP-I might protect against oxidative stress induced by H_2O_2 by activating Nrf2-mediated antioxidant pathway.

4. Conclusion

According to the results of RSM, the MPMA were extracted by 60% ethanol, 140 min, 85°C, and liquid-to-solid ratio of 30 mL/g. After purification with macroporous resin HPD600, the samples were MPMAP-I, MPMAP-II,

MPMAP-III, and the TPC contents were 423, 413, and 228 mg/g, respectively. FT-IR results showed that the three samples differed in their chemical structures, but all had the IR characteristics of polyphenols. In the same way, the results of UPLC-MS/MS showed that there were clear differences in the types of polyphenols among the three samples, indicating that the macroporous resin HPD600 could be used to separate the compounds, which made the composition differences among the three samples evident. In addition, these three samples showed potential in vitro antioxidant activities but with different effects, and MPMAP-I had better antioxidant activities overall. MPMAP-I also showed better hepatoprotective activity than MPMAP-II and MPMAP-III, which may be related to its more abundant compounds or content. Cell experiments showed that MPMAP-I had a better hepatoprotective effect. L02 cells pretreated with different concentrations of MPMAP-I showed a certain resistance to oxidative stress induced by H_2O_2. The results showed that MPMAP-I might inhibit the overexpression of p53, increase the ratio of Bcl-2/Bax, and eventually interfere with the activation of the caspase-3 cascade to inhibit H_2O_2-induced apoptosis. At the same time, MPMAP-I might also protect against H_2O_2-induced oxidative stress by activating the Nrf2-mediated antioxidant pathway. The above experimental results also could be validated by further research, to clarify the molecular mechanisms of observed biological activities.

While our earlier preprint [44] highlighted the protective effects of MPMA polyphenols against H_2O_2-induced liver injury in L02 cells, the exact composition of these polyphenols was not identified. In this study, UPLC-MS/MS analysis allowed us to pinpoint the specific components of each fraction, paving the way for future in-depth investigations into individual compounds. At present, there are not many in vivo studies of MPMA. Early studies showed that MPMA extracts were shown to have antioxidant, antiatherogenic, and choleretic effects in animal experiments and clinical observations [16]. In addition, MPMA extract has been used to reduce liver injury and lipid accumulation in NAFLD rats, but the preparation process of the extract has not been given [45]. Recent studies have found that MPMA polyphenols can inhibit oxidative stress in diabetic mice by activating Keap1/Nrf2/ARE signaling pathway [46]. These results indirectly supported the potential in vivo antioxidant and body protective effects of the components in this study. Our study provides the specific preparation process and component analysis of the extract, which is conducive to further in vivo studies of related active substances. Further research is needed to elucidate the molecular mechanisms underlying the observed biological activities and to explore the potential therapeutic applications of MPMA polyphenols in oxidative stress–related liver diseases.

Nomenclature

Bax	Bcl-2-associated X protein
Bcl-2	B-cell lymphoma-2
CAT	Catalase
CV	Coefficient of variation
DMEM	Dulbecco's modified Eagle's medium
FBS	Fetal bovine serum
FRAP	Ferric reducing antioxidant power
GOT	Glutamic oxaloacetic transaminase
GPT	Glutamic pyruvic transaminase
GPx	Glutathione peroxidase
MDA	Malondialdehyde
MMP	Mitochondrial membrane potential
MPMA	*Mallotus peltatus* (Geiseler) Mull. Arg.
NAFLD	Nonalcoholic fatty liver disease
NASH	Nonalcoholic steatohepatitis
Nrf2	Nuclear factor erythroid 2–related factor 2
PBS	Phosphate-buffered saline
PS	Phosphatidylserine
ROS	Reactive oxygen species
RSM	Response surface method
SOD	Superoxide dismutase
TPC	Total phenolic content
γ-GCL	γ-Glutamylcysteine ligase

Data Availability Statement

The data that support the findings of this study are available from the corresponding author upon reasonable request.

Disclosure

This manuscript was previously available as a preprint on the Social Science Research Network (https://doi.org/10.2139/ssrn.4873480) on June 27, 2024.

Conflicts of Interest

The authors declare no conflicts of interest.

Author Contributions

Ying-Jing Zhang and Jin-Xin Li carried out experiments, analyzed data, and wrote the manuscript. Ke-Xin Hao, Rui-Fang Zhong, and Yi-Meng Li provided experimental and paper revision guidance. Jian-Guo Jiang and Wei Zhu supervised and edited the project. All authors read and approved the final manuscript. Ying-Jing Zhang and Jin-Xin Li contributed to the work equally and should be regarded as co-first authors.

Funding

This project was supported by the National Natural Science Foundation of China (32072201 and 32372286), Natural Science Foundation of Guangdong Province (2023A1515011967 and 2023A1515012223), Foshan City Science and Technology Tackling Special Project in Social Areas (2120001008478), and National Natural Foundation of China (82374239) and Guangzhou Science and Technology Plan Project (202201011762).

Acknowledgments

The authors appreciate the insightful feedback received from both the scientific community and reviewers during the preprint phase.

This project was supported by the National Natural Science Foundation of China (32072201 and 32372286), Natural Science Foundation of Guangdong Province (2023A1515011967 and 2023A1515012223), Foshan City Science and Technology Tackling Special Project in Social Areas (2120001008478), and National Natural Foundation of China (82374239) and Guangzhou Science and Technology Plan Project (202201011762).

Supporting Information

Additional supporting information can be found online in the Supporting Information section. *(Supporting Information)*

The Supporting Information includes additional figures and data supporting the findings presented in this study. These include the Chromatography of MPMAP-1, MPMAP-II, and MPMAP-III (Figure S1), and the table of single factor experimental design (Table S1), central composite design (Table S2), and primer sequences used in RT-qPCR analysis (Table S3).

References

[1] P. Farzanegi, A. Dana, Z. Ebrahimpoor, M. Asadi, and M. A. Azarbayjani, "Mechanisms of Beneficial Effects of Exercise Training on Non-Alcoholic Fatty Liver Disease (NAFLD): Roles of Oxidative Stress and Inflammation," *European Journal of Sport Science* 19, no. 7 (2019): 994–1003, https://doi.org/10.1080/17461391.2019.1571114.

[2] A. Paoli and G. Cerullo, "Investigating the Link Between Ketogenic Diet, NAFLD, Mitochondria, and Oxidative Stress: A Narrative Review," *Antioxidants* 12, no. 5 (2023): 1065, https://doi.org/10.3390/antiox12051065.

[3] C.-C. Zhong, T. Zhao, C. Hogstrand, F. Chen, C.-C. Song, and Z. Luo, "Copper (Cu) Induced Changes of Lipid Metabolism Through Oxidative Stress-Mediated Autophagy and Nrf2/PPARγ Pathways," *The Journal of Nutritional Biochemistry* 100 (2022): 108883, https://doi.org/10.1016/j.jnutbio.2021.108883.

[4] S. Raza, S. Rajak, A. Upadhyay, A. Tewari, and R. A. Sinha, "Current Treatment Paradigms and Emerging Therapies for NAFLDNASH," *Frontiers in Bioscience* 26, no. 2 (2021): 206–237, https://doi.org/10.2741/4892.

[5] A. Takaki, D. Kawai, and K. Yamamoto, "Multiple Hits, Including Oxidative Stress, as Pathogenesis and Treatment Target in Non-Alcoholic Steatohepatitis (NASH)," *International Journal of Molecular Sciences* 14, no. 10 (2013): 20704–20728, https://doi.org/10.3390/ijms141020704.

[6] M. N. Park, M. A. Rahman, M. H. Rahman, et al., "Potential Therapeutic Implication of Herbal Medicine in Mitochondria-Mediated Oxidative Stress-Related Liver Diseases," *Antioxidants* 11, no. 10 (2022): 2041, https://doi.org/10.3390/antiox11102041.

[7] M. Moorthy, U. Sundralingam, and U. D. Palanisamy, "Polyphenols as Prebiotics in the Management of High-Fat Diet-Induced Obesity: A Systematic Review of Animal Studies," *Foods* 10, no. 2 (2021): 299, https://doi.org/10.3390/foods10020299.

[8] W. Yuan, M. Zhang, C. Wang, et al., "Resveratrol Attenuates High-Fat Diet–Induced Hepatic Lipotoxicity by Upregulating Bmi-1 Expression," *Journal of Pharmacology and Experimental Therapeutics* 381, no. 2 (2022): 96–105, https://doi.org/10.1124/jpet.121.001018.

[9] M. Yamamoto, Y. Yoshioka, T. Kitakaze, Y. Yamashita, and H. Ashida, "Preventive Effects of Black Soybean Polyphenols on Non-Alcoholic Fatty Liver Disease in Three Different Mouse Models," *Food & Function* 13, no. 2 (2022): 1000–1014, https://doi.org/10.1039/d1fo03541j.

[10] Z. Li, H. Zhang, Y. Li, et al., "Phytotherapy Using Blueberry Leaf Polyphenols to Alleviate Non-Alcoholic Fatty Liver Disease Through Improving Mitochondrial Function and Oxidative Defense," *Phytomedicine* 69 (2020): 153209, https://doi.org/10.1016/j.phymed.2020.153209.

[11] M. Rahimlou, G. Baghdadi, A. Khodi, et al., "Polyphenol Consumption and Nonalcoholic Fatty Liver Disease Risk in Adults," *Scientific Reports* 14, no. 1 (2024): 6752, https://doi.org/10.1038/s41598-024-57416-0.

[12] P. Bag, D. Chattopadhyay, H. Mukherjee, et al., "Anti-Herpes Virus Activities of Bioactive Fraction and Isolated Pure Constituent of Mallotus Peltatus: An Ethnomedicine from Andaman Islands," *Virology Journal* 9, no. 1 (2012): 98, https://doi.org/10.1186/1743-422x-9-98.

[13] D. Chattopadhyay, G. Arunachalam, A. B. Mandal, T. K. Sur, S. C. Mandal, and S. K. Bhattacharya, "Antimicrobial and Anti-Inflammatory Activity of Folklore: Mallotus Peltatus Leaf Extract," *Journal of Ethnopharmacology* 82, no. 2-3 (2002): 229–237, https://doi.org/10.1016/s0378-8741(02)00165-4.

[14] J. Chen, X. Zhang, D. Huo, et al., "Preliminary Characterization, Antioxidant and α-Glucosidase Inhibitory Activities of Polysaccharides From Mallotus Furetianus," *Carbohydrate Polymers* 215 (2019): 307–315, https://doi.org/10.1016/j.carbpol.2019.03.099.

[15] S. Yu, Z. Duan, P. Li, et al., "Protective Effect of Polyphenols Purified From Mallotus Oblongfolius on Ethanol-Induced Gastric Mucosal Injury by Regulating Nrf2 and MAPKs Pathways," *Antioxidants* 11, no. 12 (2022): 2452, https://doi.org/10.3390/antiox11122452.

[16] L. Yueli, W. Liqun, W. Haitao, L. Lianbo, and Y. Xinan, "Comparison of Anti–Atherosclerotic Effects of Two Different Extracts From Leaves of Mallotus Furetianus," *Asian Pacific Journal of Tropical Medicine* 4, no. 11 (2011): 878–882, https://doi.org/10.1016/s1995-7645(11)60212-5.

[17] D. Chattopadhyay, G. Arunachalam, S. C. Mandal, R. Bhadra, and A. B. Mandal, "CNS Activity of the Methanol Extract of *Mallotus peltatus* (Geist) Muell Arg. Leaf: An Ethnomedicine of Onge," *Journal of Ethnopharmacology* 85, no. 1 (2003): 99–105, https://doi.org/10.1016/s0378-8741(02)00379-3.

[18] A. Ciric, B. Krajnc, D. Heath, and N. Ogrinc, "Response Surface Methodology and Artificial Neural Network Approach for the Optimization of Ultrasound-Assisted Extraction of Polyphenols from Garlic," *Food and Chemical Toxicology* 135 (2020): 110976, https://doi.org/10.1016/j.fct.2019.110976.

[19] X. Wang, X. Liu, N. Shi, et al., "Response Surface Methodology Optimization and HPLC-ESI-QTOF-MS/MS Analysis on Ultrasonic-Assisted Extraction of Phenolic Compounds From Okra (*Abelmoschus esculentus*) and Their Antioxidant Activity," *Food Chemistry* 405 (2023): 134966, https://doi.org/10.1016/j.foodchem.2022.134966.

[20] P. Chen, Y. Zhu, Y. Men, Y. Zeng, and Y. Sun, "Purification and Characterization of a Novel Alginate Lyase From the Marine Bacterium *Bacillus* sp. Alg07," *Marine Drugs* 16, no. 3 (2018): 86, https://doi.org/10.3390/md16030086.

[21] L. Sun, J. Sun, L. Chen, P. Niu, X. Yang, and Y. Guo, "Preparation and Characterization of Chitosan Film

Incorporated With Thinned Young Apple Polyphenols as an Active Packaging Material," *Carbohydrate Polymers* 163 (2017): 81–91, https://doi.org/10.1016/j.carbpol.2017.01.016.

[22] J.-J. Zhu, J.-J. Yang, G.-J. Wu, and J.-G. Jiang, "Comparative Antioxidant, Anticancer and Antimicrobial Activities of Essential Oils From Semen Platycladi by Different Extraction Methods," *Industrial Crops and Products* 146 (2020): 112206, https://doi.org/10.1016/j.indcrop.2020.112206.

[23] C.-Y. Shen, T.-X. Wang, X.-M. Zhang, and J.-G. Jiang, "Various Antioxidant Effects Were Attributed to Different Components in the Dried Blossoms of *Citrus aurantium* L. Var. Amara Engl," *Journal of Agricultural and Food Chemistry* 65, no. 30 (2017): 6087–6092, https://doi.org/10.1021/acs.jafc.7b02244.

[24] J. Chen, L. Li, X. Zhang, et al., "Structural Characterization of Polysaccharide From Centipeda Minima and its Hypoglycemic Activity Through Alleviating Insulin Resistance of Hepatic HepG2 Cells," *Journal of Functional Foods* 82 (2021): 104478, https://doi.org/10.1016/j.jff.2021.104478.

[25] Y. Yao, Z. Li, B. Qin, X. Ju, and L. Wang, "Evaluation of the Intracellular Lipid-Lowering Effect of Polyphenols Extract From Highland Barley in HepG2 Cells," *Food Science and Human Wellness* 13, no. 1 (2024): 454–461, https://doi.org/10.26599/fshw.2022.9250039.

[26] T. Yan, F. Ding, Y. Zhang, et al., "Astaxanthin Inhibits H2O2-Induced Excessive Mitophagy and Apoptosis in SH-Sy5y Cells by Regulation of Akt/mTOR Activation," *Marine Drugs* 22, no. 2 (2024): 57, https://doi.org/10.3390/md22020057.

[27] D. Qin, F. Yang, Z. Hu, et al., "Peptide T8 Isolated From Yak Milk Residue Ameliorates H2O2-Induced Oxidative Stress Through Nrf2 Signaling Pathway in HUVEC Cells," *Food Bioscience* 44 (2021): 101408, https://doi.org/10.1016/j.fbio.2021.101408.

[28] M. Muhaxi, F. Liu, and T. B. Ng, "Structural Characterization and In Vitro Hepatoprotective Activity of a Novel Antioxidant Polysaccharide From Fruiting Bodies of the Mushroom Pleurotus Ferulae," *International Journal of Biological Macromolecules* 243 (2023): 125124, https://doi.org/10.1016/j.ijbiomac.2023.125124.

[29] B. He, F. Wu, L. Fan, et al., "Carboxymethylated Chitosan Protects Schwann Cells Against Hydrogen Peroxide-Induced Apoptosis by Inhibiting Oxidative Stress and Mitochondria Dependent Pathway," *European Journal of Pharmacology* 825 (2018): 48–56, https://doi.org/10.1016/j.ejphar.2018.02.024.

[30] S. Neel, A. Mandal, A. Dutta, et al., "Response Surface Methodology Guided Process Optimizations, Modeling and Biofunctional Analysis of Phytochemicals From Nigella Sativa Seeds as a Potential Antifungal Agent," *Industrial Crops and Products* 199 (2023): 116695, https://doi.org/10.1016/j.indcrop.2023.116695.

[31] S. Nipornram, W. Tochampa, P. Rattanatraiwong, and R. Singanusong, "Optimization of Low Power Ultrasound-Assisted Extraction of Phenolic Compounds from Mandarin (Citrus Reticulata Blanco Cv. Sainampueng) Peel," *Food Chemistry* 241 (2018): 338–345, https://doi.org/10.1016/j.foodchem.2017.08.114.

[32] A. B. Legesse, S. A. Emire, M. G. Tadesse, et al., "Optimization of Ultrasound-Assisted Extraction of Verbascum Sinaiticum Leaves: Maximal Phenolic Yield and Antioxidant Capacity," *Foods* 13, no. 8 (2024): 1255, https://doi.org/10.3390/foods13081255.

[33] Y. Peng, K. S. Bishop, and S. Y. Quek, "Extraction Optimization, Antioxidant Capacity and Phenolic Profiling of Extracts From Flesh, Peel and Whole Fruit of New Zealand Grown Feijoa Cultivars," *Antioxidants* 8, no. 5 (2019): 141, https://doi.org/10.3390/antiox8050141.

[34] Y. Ma, H. Zhao, Q. Ma, et al., "Development of Chitosan/Potato Peel Polyphenols Nanoparticles Driven Extended-Release Antioxidant Films Based on Potato Starch," *Food Packaging and Shelf Life* 31 (2022): 100793, https://doi.org/10.1016/j.fpsl.2021.100793.

[35] M. A. Khan, C. Yue, Z. Fang, et al., "Alginate/Chitosan-Coated Zein Nanoparticles for the Delivery of Resveratrol," *Journal of Food Engineering* 258 (2019): 45–53, https://doi.org/10.1016/j.jfoodeng.2019.04.010.

[36] X. Chang, C.-Y. Shen, and J.-G. Jiang, "Structural Characterization of Novel Arabinoxylan and Galactoarabinan From Citron With Potential Antitumor and Immunostimulatory Activities," *Carbohydrate Polymers* 269 (2021): 118331, https://doi.org/10.1016/j.carbpol.2021.118331.

[37] M. K. Remanan and F. Zhu, "Encapsulation of Rutin Using Quinoa and Maize Starch Nanoparticles," *Food Chemistry* 353 (2021): 128534, https://doi.org/10.1016/j.foodchem.2020.128534.

[38] M. A. Kalas, L. Chavez, M. Leon, P. T. Taweesedt, and S. Surani, "Abnormal Liver Enzymes: A Review for Clinicians," *World Journal of Hepatology* 13, no. 11 (2021): 1688–1698, https://doi.org/10.4254/wjh.v13.i11.1688.

[39] X. Chen, M. Shen, J. Yang, et al., "RNA-Seq Based Elucidation of Mechanism Underlying Mesona Chinensis Benth Polysaccharide Protected H2O2-Induced Oxidative Damage in L02 Cells," *Food Research International* 157 (2022): 111383, https://doi.org/10.1016/j.foodres.2022.111383.

[40] L. Chen, F. Zhang, D. Kong, et al., "Saikosaponin D Disrupts Platelet-Derived Growth Factor-β Receptor/p38 Pathway Leading to Mitochondrial Apoptosis in Human LO2 Hepatocyte Cells: A Potential Mechanism of Hepatotoxicity," *Chemico-Biological Interactions* 206, no. 1 (2013): 76–82, https://doi.org/10.1016/j.cbi.2013.08.006.

[41] E. A. Slee, C. Adrain, and S. J. Martin, "Executioner Caspase-3, 6, and 7 Perform Distinct, Non-Redundant Roles During the Demolition Phase of Apoptosis," *Journal of Biological Chemistry* 276, no. 10 (2001): 7320–7326, https://doi.org/10.1074/jbc.m008363200.

[42] O. Al-Sawaf, T. Clarner, A. Fragoulis, et al., "Nrf2 in Health and Disease: Current and Future Clinical Implications," *Clinical Science* 129, no. 12 (2015): 989–999, https://doi.org/10.1042/cs20150436.

[43] D. Xu, M. Xu, S. Jeong, et al., "The Role of Nrf2 in Liver Disease: Novel Molecular Mechanisms and Therapeutic Approaches," *Frontiers in Pharmacology* 9 (2018): 1428, https://doi.org/10.3389/fphar.2018.01428.

[44] Y.-J. Zhang, K.-X. Hao, J.-G. Jiang, and W. Zhu, "The Polyphenols from Mallotus Peltatus (Geiseler) Mull. Arg. Protect Against H2O2-Induced Liver Injury in L02 Cells," *Heliyon* (2024).

[45] D. Lin, Y. Ding, Y. Cheng, et al., "Efficacy and Mechanism of Mallotus Furetianus Müll. Arg. Extract on Nonalcoholic Fatty Liver Disease," *Evidence-based Complementary and Alternative Medicine* 2022 (2022): 1–12, https://doi.org/10.1155/2022/4897463.

[46] M. Zhao, K. Meng, M. Zhao, et al., "Partridge Tea Polyphenols Alleviated STZ-Induced Diabetic Nephropathy by Regulating Keap1/Nrf2/ARE Signaling Pathway in C57BL/6 Mice," *Journal of Functional Foods* 115 (2024): 106127, https://doi.org/10.1016/j.jff.2024.106127.